Journal of Hydrology: Regional Studies 52 (2024) 101714

Contents lists available at ScienceDirect

Journal of Hydrology: Regional Studies

journal homepage: www.elsevier.com/locate/ejrh

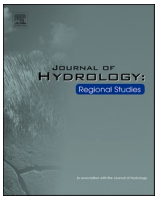

Temporal dynamics of inundation area, hydrochemistry and brine in Bakhtegan Lake, South-Central Iran

Maryam Vahidipour [a], Ezzat Raeisi [a,*], Sjoerd E.A.T.M van der Zee [b]

[a] Department of Earth science, School of Science, Shiraz University, Shiraz 7146713565, Islamic Republic of Iran
[b] Soil Physics and Land Management Group, Wageningen University, P.O. Box 47, 6700 AA, the Netherlands

ARTICLE INFO

Keywords:
Landsat
Solute geochemistry
Major ions trends
Evaporation sequence
Bakhtegan Lake

ABSTRACT

Study region: Bakhtegan Lake, southern Iran, is a "Wetland of International Importance" (Ramsar Site).
Study focus: This study focuses on analyzing the time series of the lake's inundation area, identifying factors contributing to its shrinkage, and studying its hydrochemical characteristics. To map the inundation area, Landsat images from 1972 to 2019 were used and 64 water samples were collected from the lake during 2017–2019 for geochemical modeling.
New hydrological insights for the region: The study reveals that the Bakhtegan Lake has become a seasonal lake with a long-term dry state since 2007. The lake's inundation area shows a significant correlation with the Kor River discharge, and the main reason for the lake's shrinkage is a decrease in river inflow due to over-exploitation in the basin and construction of two new dams since 2007. The lake water and brine below the lake bed have TDS concentrations varying between 70000 and 451000 mg/L and 118000–373000 mg/L, respectively. The Gibbs, Na-normalized ratio end-member diagrams show that the lake water chemistry is mainly controlled by evaporation. The saturation index indicates that brine samples were in an equilibrium state with gypsum, halite, and glauberite. The Spencer diagram and evolutionary pathway model suggest that water samples shifted toward natural sulfate-rich minerals during evaporation. The lake water evolution model predicts precipitation of halite, kieserite, and carnallite minerals during progressive evaporation.

1. Introduction

Playas, or dried lakes, often occur in semi-arid and arid climates due to a negative balance between evaporation and precipitation (Yechieli and Wood, 2002). Recently, over 70% of lake shrinkages have occurred in Asia, especially in the Middle-East, due to human activities and drought (Micklin, 2016). These lakes are experiencing ecological changes due to both natural and anthropogenic activities. Numerous studies have discussed the main factors contributing to lake shrinkages worldwide. Effective monitoring of lake inundation areas helps to understand the causes of degradation. Recently, remote sensing, specifically the Landsat-series satellites, has been used extensively to monitor the long-term dynamics of lake extents (Zhu et al., 2022). The normalized difference water index (NDWI) is widely applied to study lake inundation areas (Liu et al., 2018; Zhou et al., 2019; Wang et al., 2022). Cao et al. (2021) applied Landsat series satellite remote sensing data from 1973 to 2019 in combination with the NDWI water body index threshold

* Corresponding author.
E-mail address: e_raeisi@yahoo.com (E. Raeisi).

https://doi.org/10.1016/j.ejrh.2024.101714
Received 24 September 2023; Received in revised form 30 January 2024; Accepted 20 February 2024
Available online 27 February 2024

method to obtain a 46-year area dataset for the Hongjiannao Lake. Their results showed that the shrinkage of the Hongjiannao Lake is mainly caused by anthropogenic factors, followed by natural factors.

Hydrochemical investigations on diminished lakes offer vital insights into ecological changes, hydrochemical reactions, and the processes that govern them. However, research on hydrochemistry on shrunken lakes with extreme evaporitic conditions is relatively rare. The sources of salinity were determined by measuring major ions and stable isotopes, such as $\delta^{18}O$ and $\delta^{2}H$ (Fan et al., 2018; Franco et al., 2020). Khosravi et al. (2018) studied the chemical evolution of brine in Maharlu Lake, Iran, during both wet and dry seasons. Their findings revealed that the degree of evaporation and the precipitation-dissolution of salt minerals in the lake bed are the primary factors influencing the chemical compositions of the lake water and sediment pores.

Otálora et al. (2020) studied the evaporation sequence in Salar de Atacama, Chile, using a combination of in-situ, laboratory, and modeling techniques. Their findings revealed that the brines exhibit density stratification, with significant gradients in salinity, temperature, pH, dissolved oxygen, and oxidation-reduction potential. These vertical gradients, as well as lateral and seasonal variations, are the primary factors influencing chemical variability and controlling precipitation processes. Furthermore, evaporation of these brines results in chemical transformation of various ions and leads to the formation of macrocrystalline gypsum precipitates surrounded by a crystalline crust composed of chlorides, sulfates, and borates.

Iran has abundant wetland resources, with 25 sites designated as "Wetlands of International Importance" (Ramsar Sites), covering a vast surface area of 1.488 million hectares. Among these sites are the Bakhtegan and Tashk Lakes in south-central Iran, ranking as the second-largest inland lakes (Fig. 1). The lakes and their surrounding marshes were officially recognized by the Ramsar Convention as the Neiriz Lakes and Kamjan Marshes in 1975 and became a national park in 1995 (Ramsar Convention, 2023).

In addition, the Bakhtegan and Tashk lakes have been designated in the Montreux Record since 1990, with the risk that their ecological character will change.

The Bakhtegan-Tashk national park is home to a diverse range of wildlife, including 86 mammal species, 218 bird species, 30 reptile species, and 23 fish species (Fotooli, 2002). During the winter season, the lakes serve as a temporary habitat for 95 migratory bird species from the Caspian Sea, Lake Urmia, and Siberia. The water supply for the Bakhtegan and Tashk Lakes primarily comes from the perennial Kor River. Noori et al. (2021) concluded that the Bakhtegan basin is a hotspot with respect to groundwater depletion in Iran. However, due to excessive groundwater extraction from agricultural wells, diversion of the Kor River through new channels, and the construction of Mollasadra and Sivand reservoirs, the Bakhtegan and Tashk Lakes have experienced significant shrinkage since 2007. This, combined with drought conditions, has transformed the once-permanent lake into a seasonal one (Vahidipour et al., 2021). In the wet season, the deep parts of the lakes receive water through rainfall and flood events. The study area exhibits a pan evaporation rate that is 11.8 times higher than the precipitation rate. As a consequence, the lakes completely disappear during the dry season due to the intense process of evaporation, leading to the formation of a salt crust that covers more than 74% of the lake's surface (Mohammadi

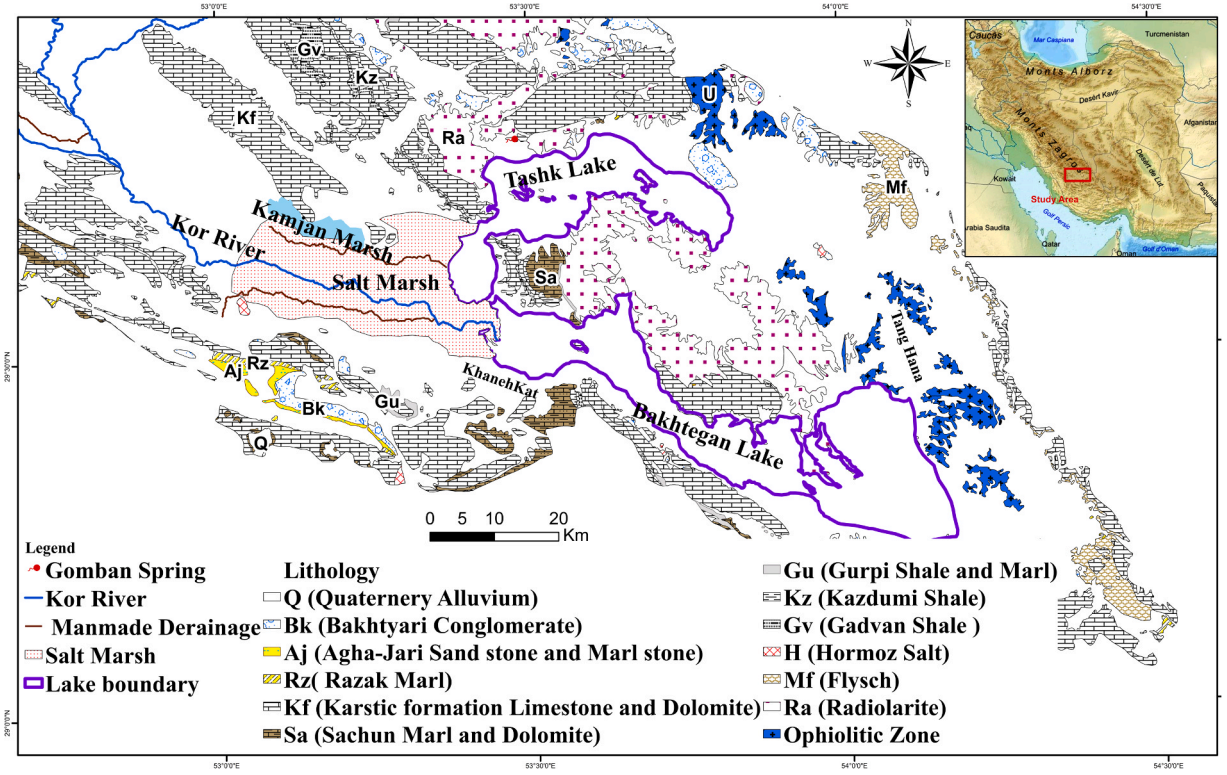

Fig. 1. Geological map of the Bakhtegan-Tashk Lakes.

et al., 2020). The dissolution of salt deposits causes extreme salinity in the lake water and groundwater below the lake beds. The average TDS (total dissolved solids) of the lake water has increased from 45,000 mg/L in 2007–256,000 mg/L in 2018 (Vahidipour et al., 2021). The main factors contributing to the rising TDS since 2007 include the decreased the Bakhtegan Lake inflow as a result of drought, the construction of two dams in the Bakhtegan Lake catchment area which restrict inflow into the Bakhtegan Lake, and the excessive exploitation of aquifers by wells in both the Bakhtegan Lake catchment area and coastal regions.

The shrinkage of the Bakhtegan has led to high concentrations of As, Mo and Hg in the sediment and water of the lake (Vahidipour et al., 2022). Saline lake water and groundwater in the sediments flow from the lake toward the adjacent coastal aquifers (Vahidipour et al.,2021). Salinity measurements of agricultural wells along the shoreline parts of the coastal aquifers show concentrations higher than 13000 mg/L. Active brine intrusion occurs in the coastal aquifers due to the aggressive landward groundwater flow direction (Vahidipour et al., 2021).

No systematic investigations have been conducted yet regarding the shrinkage of the Bakhtegan Lake. The hydrochemistry of the lake has not been extensively studied. Löffler (1961) conducted a limnological study and measured the major ions of the lake water. Further research is needed to understand the hydrochemistry of lake water after shrinkage and evaporate mineral changes sequence through time series measurements. The objectives of this study are: (i) to extract annual lake maps of the Bakhtegan Lake from 1972 to 2019 using a water indices-based water body mapping algorithm, all the available Landsat images, and the cloud computing platform ENVI software, (ii) to investigate the underlying causes of changes in lakes including both natural and anthropogenic factors, (iii) to conduct a comprehensive analysis to assess the origin, and the hydrochemical characteristics of the water and their controlling factors, and finally, (iv) to assess the evolution of evaporation brine using a combination of field data and hydrochemistry thermodynamics modeling to determine the sequence of minerals based on measured data modeling. This study aims to provide a better understanding of the composition and evolution of the Bakhtegan Lake, which serves as an example of a closed system in an arid environment.

2. Study area

2.1. Geology

The Bakhtegan Lake (29∘13′ to 29∘50′ N and 53∘15′ to 54∘10′ E) is situated in Fars Province, southern Iran (Fig. 1). Based on sedimentary, tectonic, and magmatic characteristics, it is positioned between two regions, namely the High Zagros Zone and the Ophiolitic Zone. The High Zagros Thrust Belt is approximately 80 km wide and is bounded by the High Zagros Fault and the Main Zagros Thrust (Berberian, 1995). The northern, southern, and western parts of the study area are predominantly composed of karstic formations such as dolomite and limestone, while the central and eastern parts consist of Ophiolitic rocks (Fig. 1). In the dry months, the surface crust of Bakhtegan-Tashk Lakes bed can be classified into five categories, going from the center to the coast respectively: pure salt, clay salt, salty soil, soil without salt, and sand dunes (Mohammadi, 2020).

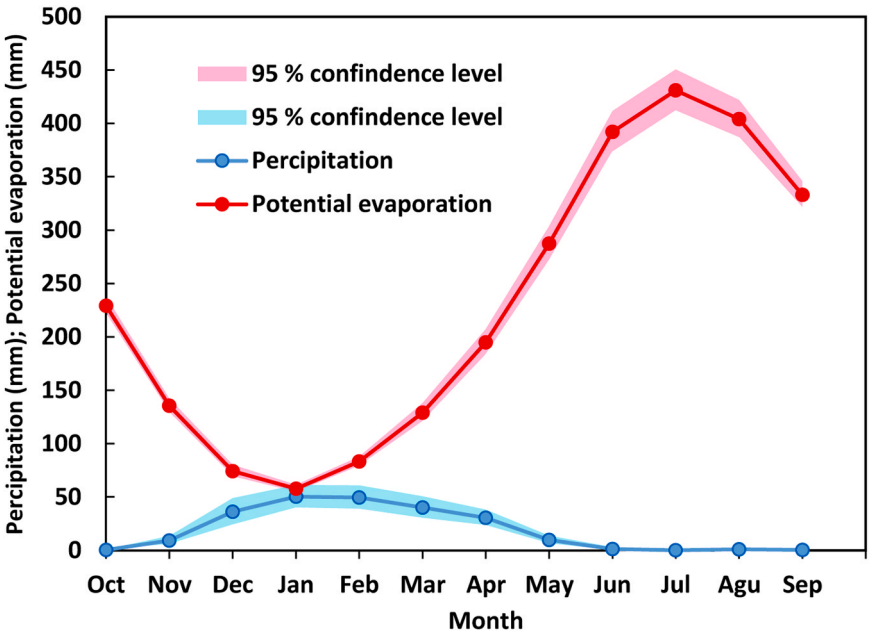

Fig. 2. Monthly variation of average rainfall from 1968 to 2018 and potential evaporation from 1976 to 2018 at the study area.

2.2. Hydrology

The Tashk and Bakhtegan lakes, along with their catchment areas, cover approximately 410, 850, and 27180 km^2, respectively. The only river that recharges the lake is the Kor River. The elevation of the study area ranges from 1543 to 2930 m above sea level (m.a.s.l). The Bakhtegan Lake experiences an arid climate with an average annual precipitation of 232 mm, ranging from 68 to 441 mm. The average annual pan evaporation is 2750 mm and the average air temperature is 19°C. Precipitation primarily occurs between November and May, while the minimum rainfall is observed from June to October. Fig. 2 illustrates the monthly mean rainfall variability from 1968 to 2018 and the potential evaporation from 1976 to 2018 in the study region. Potential evaporation consistently exceeds rainfall, particularly during the dry season. The dryness value, obtained by dividing potential evaporation by precipitation, was 11.8, indicating extensive evaporation in the study area.

The annual average discharge of the Kor River into the Bakhtegan Lake was 13.6 m^3/s between 1997 and 2007. However, since 2007, the annual average discharge has significantly decreased to 0.9 m^3/s due to groundwater overexploitation, drought, and the construction of two new dam reservoirs in the Kor River basin (Vahidipour et al., 2021). The Doroudzan, Mollasadra, and Sivand

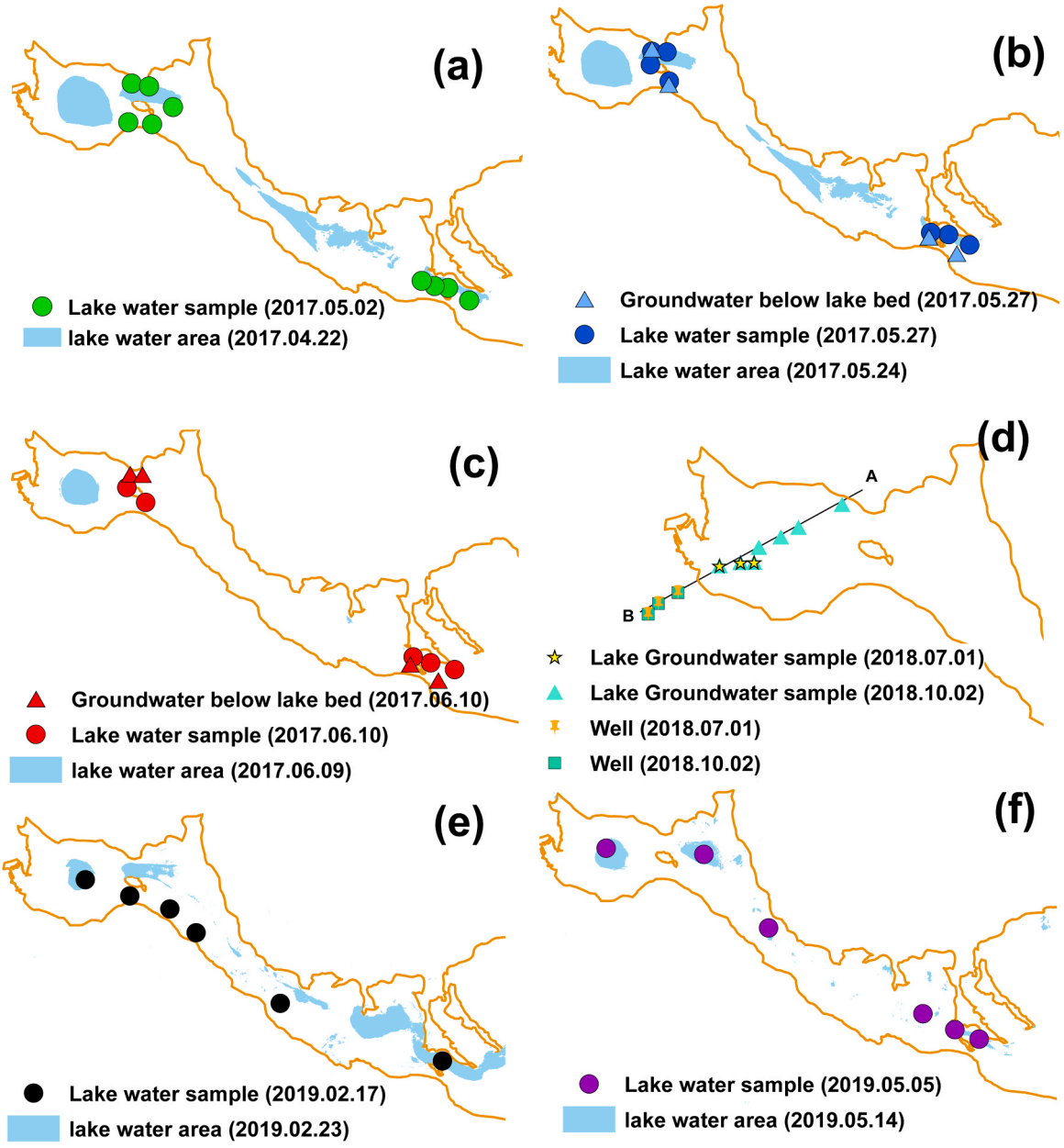

Fig. 3. Water sampling sites and lake water areas in the different sampling periods.

reservoir dams, were built in the Kor River basin in 1972, 2006, and 2006, respectively, with a total effective capacity of 1285 million m^3. Numerous diversion channels divert water from the Kor River for agricultural purposes throughout its branches. Six old diversion dams have converted the downstream basin into farmland, but currently, no water is being carried due to upstream overexploitation (Torabi et. al, 2017). The primary water sources for the Bakhtegan Lake are the Kor River directly, a channel in the southern Kor River, and various natural drains from the adjacent highlands. The Kamjan Marsh area covers 100 km^2 and consists of both perennial and seasonal marshes along the Kor River. However, extensive drainage of the marsh for rice farming has resulted in the conversion of a large portion of the Kamjan Marshes into agricultural land since 1967. Approximately 52.5 km^2 of the Kamjan Marsh remains intact (Vahidipour et al., 2021).

3. Materials and methods

3.1. Lake-surface area mapping

Numerous studies have utilized satellite images to effectively monitor the changes in lake inundation and hydrological fluctuations in remote regions (Adams and Sada, 2014; Scuderi et al., 2017). In this study, a total of 63 Landsat scenes from TM, ETM+, and OLI sensors were downloaded and analyzed using the United States Geological Survey (USGS) Earth Explorer platform (https://earthexplorer.usgs.gov/) for the years between 1972 and 2019. The selected Landsat scenes covered Path number: 174, Row number: 40 (1972–1982) and Path number: 162, Row number: 162 (1982–2019). To represent the dry and wet seasons in the study area, the months of October and May were chosen from the complete database to extract the areas of lake water. The downloaded scenes were preprocessed using ENVI 5.3 software, which included radiometric calibration, quick atmospheric correction (QUAC), and gap filling for Landsat 7 ETM+ scenes to minimize radiometric, atmospheric and device errors. The area of interest, the Bakhtegan Lake, was selected through spatial subset selection from each full scene.

The NDWI was utilized to identify water bodies by analyzing green and NIR wavelengths, as defined by McFeeters (1996). The formula for NDWI calculation is as follows:

$$\mathrm{NDWI} = \frac{\mathrm{Green} - \mathrm{NIR}}{\mathrm{Green} + \mathrm{NIR}} \quad (1)$$

In this equation, Green and NIR represent the surface reflectance values for the green and near-infrared bands, respectively. Many studies have established threshold values for water body extraction, ranging from NDWI > 0.2 to NDWI > 0.5. A value of NDWI > 0.2 indicates shallow water, while NDWI > 0.5 represents deep water (Ismail et al., 2022; Ullah et al., 2022; Zhu et al., 2022). Considering that the Bakhtegan Lake has a maximum depth of 3 m, a threshold of NDWI > 0.2 was used to identify the lake water bodies. To track changes in the inundation area over time, polygon shapefiles were employed in ArcGIS_ v.10.3 to calculate the water body area. These processes resulted in a time series depicting the lake's inundation area with seasonal resolution over the past 47 years.

3.2. Water sample and preservation physical and chemical analyses

A total of 64 water samples were collected between May 2017 and May 2019, consisting of 36 lake water samples, 18 groundwater below lake bed samples, 8 well samples from the adjacent aquifer, and 2 spring samples (Fig. 3). The characteristics of these samples, including the sampling date, type, and number of samples, as well as the major ions and TDS, are presented in Table1 and Table S1. To ensure proper storage, the water samples were placed in pre-cleaned polyethylene bottles and kept at a temperature of 4 °C in thermal boxes. Within 24 hours of sampling, the samples were transported to the laboratory for analysis.

Two water samples were collected at each sampling station. The pH of each water sample was measured on-site using a portable device (Waterproof CyberScan PCD 650 – Eutech). A total of 64 water samples were analyzed at the Hydrochemistry and Tracing Laboratory of the Department of Earth Sciences, Shiraz University, Iran, for the major ions including Na^+, K^+, Ca^{2+}, Mg^{2+}, Cl^-, HCO_3^- and SO_4^{2-}, as well as the TDS. The concentrations of Ca^{2+}, Mg^{2+} and HCO_3^- were determined using the titration method (APHA, 1998). The concentrations of Na^+, K^+ were measured using the standard F-AAS method (BWB model), while chloride contents were

Table 1
Sample dates, types, and number of samples for chemical analyses of the major ions (Ca^{2+}, Mg^{2+}, Na^+, K^+, SO_4^{2-}, HCO_3^- and Cl^-), trace elements (Li^+, Rb^+, Cs^+ and Sr^{2+}) and TDS.

Date	No of samples analysis for major ions				No of samples analysis for trace elements		
	Lake water	GW	Well	Spring	Lake water	GW	Well
05-May-2017	11			2	4		
27-May-2017	7	4	1				
10-Jun-2017	5	4	1		4	3	
01-Jun-2018		3	3				
10-Oct-2018		7	3			4	2
17-Feb-2019	7						
05-May-2019	6						

GW: groundwater below lake bed samples.

measured using Mohr's method (APHA, 1998). TDS values were obtained through the evaporation method, and SO_4^{2-} was analyzed using a spectrophotometric technique with the Hach DR/3000 Spectrophotometer (APHA, 1998).

A total of 17 water samples were analyzed for the trace elements of Li^+, Rb^+, Cs^+ and Sr^{2+}. This included 8 surface water samples, collected in the period from May 2017 to June 2017, 3 groundwater samples from below the lake bed in June 2017, 4 groundwater samples below the lake bed along transact AB from the center of Bakhtegan Lake toward the adjacent aquifer in October 2018, and 2 samples from wells in the adjacent aquifers in October 2018 (Table 1 and Fig. 3). The water samples were collected in dark polyethylene bottles that had been pre-cleaned, then filtered through a 0.45 μm filter and acidified with 65% nitric acid to achieve a pH of less than 2. The trace ions were measured using the ICP-MS method (Perkin Elmer Sciex ELAN 6100) at ACT Labs in Ontario, Canada.

3.3. Data quality assurance (QA) and quality control (QC)

To assure the quality of the chemical analyses, the ion charge balance was calculated. The ion charge balance ranged from 0.9 to 6, with an average of 3. For trace ions, QA and QC were calculated using blank reagents, duplicate samples, and the certified reference IV-STOCK-1643 for water. The precision of the evaluations, measured as the relative standard deviation, varied between 0.2% and 5% for the water samples. Standard and duplicate samples were used to assess the accuracy of the analyses. The percentage of recoveries for the water samples ranged from 96% to 110%.

3.4. Geochemical assessment methods

Piper Diagram: The Piper diagram is a ternary diagram that plots the percentage of major cation and anion concentrations in meq/L. It consists of two triangular diagrams that are projected onto a central diamond diagram (Piper, 1944). The AqQA software v 1.1.1. was used to construct the Piper diagrams for the analysis of the hydrochemical properties and the water type.

Gibbs diagram: Gibbs (1970) proposed a semi-logarithmic plot of TDS concentrations against the weight ratios of $Cl^-/(Cl^- + HCO_3^-)$ or $Na^+/(Na^+ + Ca^{2+})$ to gain insight into three major end-members controlling the surface water chemistry by analyzing many surface waters, such as river, lake, ocean and rain samples: (1) atmospheric precipitation: the low TDS values (TDS of about 10 mg/L), and high ratios of $Cl^-/(Cl^- + HCO_3^-)$ or $Na^+/(Na^+ + Ca^{2+})$ (approximating to 1); (2) evaporation-crystallization: high TDS values and high ratios of $Cl^-/(Cl^- + HCO_3^-)$ or $Na^+/(Na^+ + Ca^{2+})$ (approximating to 1); and (3) rock weathering: medium TDS values (between 70 and 300 mg/L), and low ratios of $Cl^-/(Cl^- + HCO_3^-)$ or $Na^+/(Na^+ + Ca^{2+})$ (< 0.5) (Stallard and Edmond, 1983).

Ratios of major ions: Ratios of major ions were used to identify relationships among major ions and understand geochemical processes. Data for the three-component end-members, namely carbonates, silicates, and evaporites, were obtained from Gaillard et al. (1999).

Saturation Index (SI): The SI is a method that can determine the mineralogy of water samples without analyzing the mineralogy of the solid phase (Deutsch, 2020). By measuring the saturation state of related mineral phases such as carbonates, sulfates, and chlorides, the SI provides valuable information about the evolution of water and the precipitation of minerals. Available measured data can be used to evaluate the saturation state of these mineral phases. In theory, as water evolves through processes like evaporation, the concentration of ions increases, leading to the precipitation of minerals. This precipitation typically starts with carbonates, followed by sulfates, and finally halite (Meredith et al., 2009). The SI is calculated using the following equation:

$$SI = \log\left(\frac{IAP}{K_{sp}}\right) \tag{2}$$

In the dissolution reaction, IAP represents the ionic activity product, while K_{sp} stands for the solubility product. The SI values range from -0.5 to $+ 0.5$, indicate saturation or equilibrium (Levy and Amrhein, 2011; Han et al., 2014). SI values above $+ 0.5$ indicate oversaturation and result in removal from the solution. Conversely, SI values below - 0.5 indicate unsaturation, causing minerals to dissolve in the solution (Otálora et al., 2020). The SI values of the water samples were determined using IPHREEQC v3.3.12–12704 (Parkhurst and Appelo, 2013).

Spencer diagram: To improve the distinction of brine concentration due to the occurrence of evaporation, the Spencer triangular diagram (Spencer, 2000; Li et al., 2020) was applied. This triangle represents the ternary system Ca^{2+}- SO_4^{2-} - alkalinity, based on Hardier and Eugster's "chemical divides" model (1970), which predicts the water evolution trajectory (Jones and Deocampo, 2003). A triangular diagram was constructed using the AqQA software to evaluate water evolution.

Chemical model of evaporation: For inferring the water evaporation evolution, hydrochemical investigations and simulations were conducted using IPHREEQC interactive v3.3.12–12704 (Parkhurst and Appelo, 2013) with the Pitzer database (Parkhurst and Appelo, 1999).

4. Results and discussion

4.1. Time series of the lake inundation area

Before its shrinkage, the Bakhtegan Lake existed in its natural state where the primary sources of water were the Kor River and direct floodwater flow into the lake. Additionally, the water levels of the aquifers surrounding the Kor River were higher than that of the river itself, resulting in significant amounts of groundwater seeping into the river, and ultimately, discharging into the lake. The

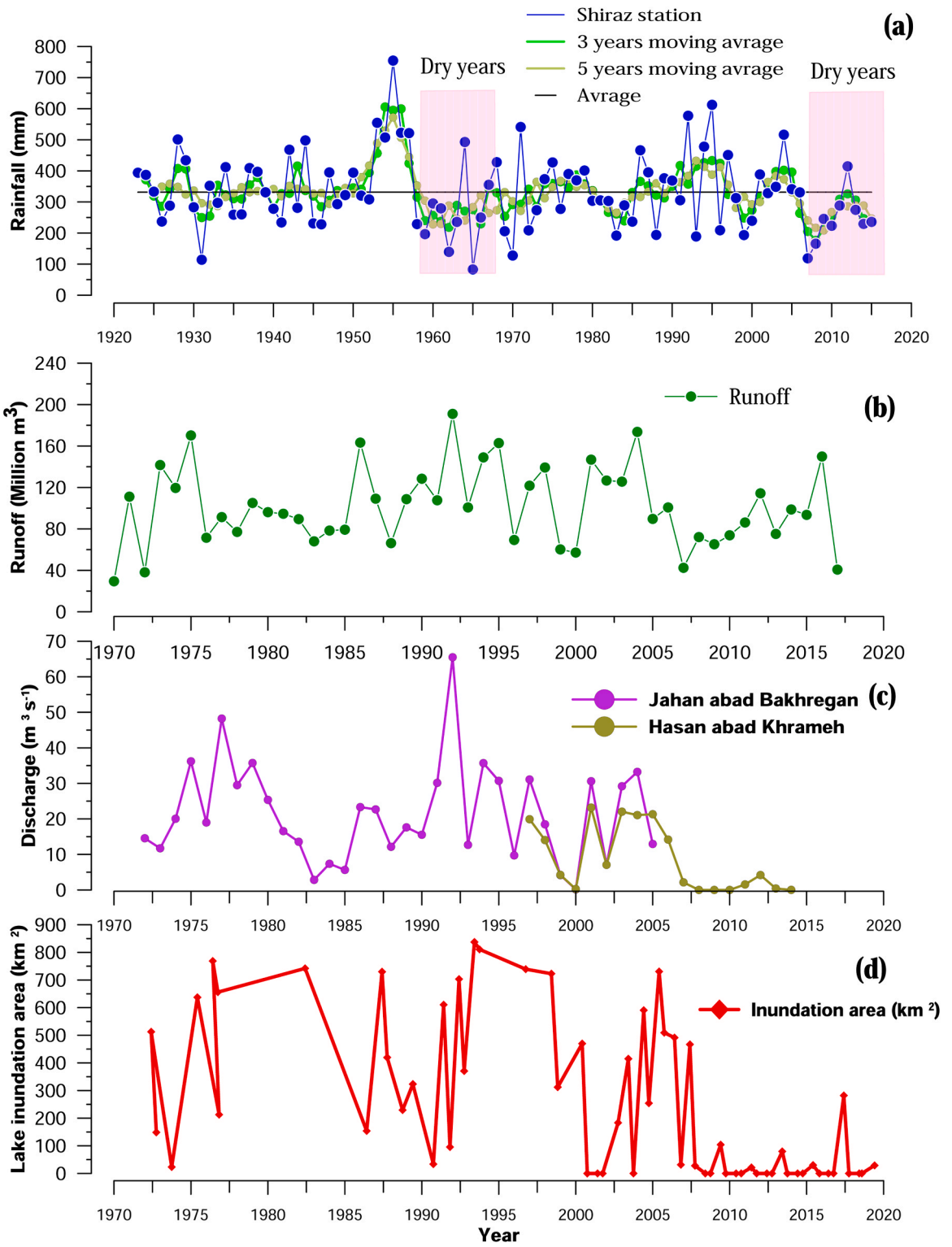

Fig. 4. (a) Precipitation at the Shiraz station from 1923 to 2015, (b) Calculated surface runoff from 1970 to 2017, (c) Kor River discharge from 1973 to 2019, and (d) The lake-surface area (km^2) curve for the Bakhtegan Lake from 1973 to 2019.

traditional dams constructed on the Kor River had a lower total effective capacity compared to the current conditions, as they were mainly used for agricultural purposes and returning water back to the river.

The fluctuation of the lake's inundation area during the wet (May) and dry (October) seasons from 1972 to 2019 is depicted in Fig. 4d. Landsat images clearly illustrate the growth and shrinkage of the lakes over time. A comparison between the lake areas in May and October reveals that the water body expands during wet seasons and contracts during dry seasons. The lake's inundation area reached its maximum surface area of approximately 837 km^2 in 1993, a wet year, but decreased to zero in October 2000, 2001 and 2003 due to dry years and drought. In the dry season, the inundation area completely dried up, while in the wet season, it was less than 50 km^2 from 2007 to 2019. Since 2007, the lake has only received direct precipitation on its surface as the discharge from the Kor River has stopped for twelve consecutive years.

4.2. Cause of the Bakhtegan Lake shrinkage

The potential factors contributing to the shrinkage of the Bakhtegan Lake include both climate change and human activities. This study considers annual precipitation as measures of climatic factors, and the construction of dams and overexploitation of groundwater in the catchment area as measures of human activities. Therefore, the main factors leading to the shrinkage of Bakhtegan Lake are discussed categorically as follows: (1) change of climate factors and drought, (2) decreasing the Kor River discharge, (3) construction of dams, and (4) overexploitation by wells.

4.2.1. Change of climate factors and drought

The precipitation time series for Shiraz meteorological station from 1923 to 2015 is depicted in Fig. 4a. The mean annual precipitation in the region is 232 mm, with a peak of 754.7 mm during 1955 – 1956, and a minimum of 82 mm during 1965–1966. While there have been several wet and dry years based on precipitation, none have been more severe than the recent droughts. The natural process of dry and wet years has been ongoing, as evidenced by the average annual rainfall of 244 mm during the dry years within the 1957 – 1958 rain-year to the 1978 – 1979 rain-year, also, average annual rainfall was 244 mm from 2007 to 2008 rain-year to 2015 – 2016 rain-year. Lake shrinkage cannot be solely attributed to climate change in the past decade, similar to the dry years from 1957 to 1982, when the Bakhtegan Lake decreased in size but did not disappear entirely. Based on the obtained data from the Bakhtegan Lake regional station, there have been no sudden or significant changes in climate factors in the study area over time.

4.2.2. Decreasing the Kor River discharge

The time series data of annual average discharge of the Kor River at Jahanabad and Hassanabad stations, which are the closest hydrometrical stations to the Bakhtegan Lake, are presented in Fig. 4b for the period from 1972 to 2019. The data shows that the Kor River discharge fluctuated in accordance with wet and dry years from 1972 to 2007. However, there was only one instance where the river discharge stopped during the dry years of 2000–2001. In 2007, the discharge of the Kor River into the Bakhtegan Lake reached almost zero, and since then, no water has entered the lake from the Kor River for the past 12 years, from 2007 to 2019.

Furthermore, the annual average Kor River discharge was compared to the lake's water inundation area from 1972 to 2019, revealing a strong correlation ($r^2 = 0.77$) between the two.

The time series of calculated runoff are presented in Fig. 4b. The maximum and minimum runoff inflow were calculated to be about 190.9 million m^3 and 29.4 million m^3 in 1994 and 1970, respectively. The river inflow has dried up since 2007, and the lake water has been mainly supplied by precipitation and surface runoff. This finding demonstrates that the peaks in the water volume increase correspond to the highest precipitation and surface runoff.

4.2.3. Construction of dams

The impoundment of two new dams, the Sivand and Mulla Sadra, began in 2006. It can be inferred that these dams led to a significant decrease in the inflow of the Kor River into the Bakhtegan Lake.

4.2.4. Overexploitation by pumping wells

Global groundwater assessments rank Iran among the countries with the highest groundwater depletion rates (Noori et al., 2021 and Maghrebi et al., 2021). The Bakhtegan basin is the most important agricultural hub in Fars province. Although the construction of dams and drought have played a role in the shrinking of Bakhtegan Lake, the main factor remains overexploitation by wells. In the years of 2004 (wet) and 2009 (dry), the discharges of wells in the basin were 2800 million m^3 and 2700 million m^3, respectively. In 2018, it decreased to 1300 million m^3. This indicates that the excessive use of agricultural wells and the direct installation of pumps on the river are the primary reasons for the complete shrinkage of the lake. These activities have caused the groundwater table to drop below the river bed, preventing groundwater from seeping into the river.

The direction of groundwater flow in the coastal aquifers of Bakhtegan Lake is shown in Fig. S1 (Vahidipour et al., 2021). In the years of 2004 (wet) and 2009 (dry), the discharges of wells in the basin were 440 million m^3 and 411 million m^3, respectively. In 2018, this further decreased to 235 million m^3. The overexploitation of aquifers adjacent to the Bakhtegan Lake has resulted in a reversal of the natural groundwater flow direction. As a result, there is no longer any groundwater flow from the coastal aquifer recharge into the lake. The indiscriminate extraction from these aquifers has caused a shift in the direction of groundwater flow, diverting it away from the lake and towards the adjacent aquifers.

4.3. Chemical composition of the Bakhtegan Lake

The concentrations of major and trace ions are presented in Table S1. The ionic balance error ranges from 0.24% to 6.2%. The content of major ions, measured in meq/L, follows the order of $Cl^- > SO_4^{2-} > HCO_3^-$ for anions and $Na^+ > Mg^{2+} > Ca^{2+} > K^+$ for cations. The TDS values of the lake water range from 70000 mg/L to 451000 mg/L, with the lowest values observed during post-rainfall sampling in March and the highest values found in the central parts of the lake where there is a maximum salt deposit, particularly pure salt and clay salt surface crusts. The TDS content increases as the salts become more concentrated in the water due to evaporation, even resulting in the disappearing of the water bodies from May to June. The TDS content of brine samples below the lake bed vary from 118000 mg/L to 373000 mg/L, gradually increasing from the shoreline towards the central parts as depth to water table decreases and evaporation effects increase. The TDS found in brine samples taken from below the lake bed are lower than those found in the lake water. This can be attributed to the diminishing effect of evaporation as the depth to the water table increases. The TDS values of wells in adjacent aquifers range between 2200 mg/L and 12900 mg/L. Saline wells are located near the shoreline in the brackish zone area, indicating that lake water infiltrates the groundwater in adjacent aquifers. On the other hand, freshwater wells are situated far from the coast and are recharged by freshwater from karstic formations. The springs had TDS concentrations ranging from 500 mg/L to 4850 mg/L. An increase in salinity observed in one of the springs suggests that it has been affected by saline water intrusion.

The hydrochemical facies and variability of water types in the samples are depicted in the Piper diagram of 1944 (Fig. 5a and b). The transition, from being fresh to becoming saline, indicates that only a few water samples remain within the freshwater zone, while the majority are subjected to salinization. Generally, the chemical compositions of the lake water, the brine beneath the lake bed, and the wells indicate Na-Cl water type. However, there are exceptions, such as one sample of lake water in June, two wells, and one spring near the shoreline, which all exhibit Mg-Cl type. The chemical composition of springs adjacent to the karstic formations is characterized by Mg-HCO_3 type. In the anion diagram, all water samples, except for one spring fall close to the Cl^- apex where Cl^- values, exceeded 80%, indicating the predominance of Cl^- in the samples. The cation plot reveals that most samples fall in the lower right corner, indicating the dominance of Na^+. In the lake water with increasing TDS, Na^+ concentration decreases and the samples shift from the Na^+ apex towards the Mg^{2+} apex due to increased evaporation intensity from May to June (Fig. 5a). This can be attributed to certain ions, such as Mg^{2+}, Li^+, K^+, Br^-, and Cl^- that behave conservatively and do not participate in salt evaporate, remaining in solution during evaporation (Brantley et al., 1984). Samples from brine below the lake bed align closely to the sodium axis. The amount of Na^+ decreases, while $Mg^{2+} + Ca^{2+}$ increases in wells from the shoreline towards the center of the aquifer, indicating the intrusion of brine below the lake bed into coastal aquifers (Fig. 5b).

4.4. Mechanisms controlling hydrochemical features

As depicted in Fig. 6, the evaporation process plays a crucial role in the development of lake water and brine beneath the lake bed samples, which exhibit high TDS and a high ratio of $Na^+/(Na^+ + Ca^{2+})$ and $Cl^-/(Cl^- + HCO_3^-)$ (approximating to 1). Generally, the lake water and brine beneath the lake bed samples fall into the upper right section of the Gibbs plot, indicating a clear influence of

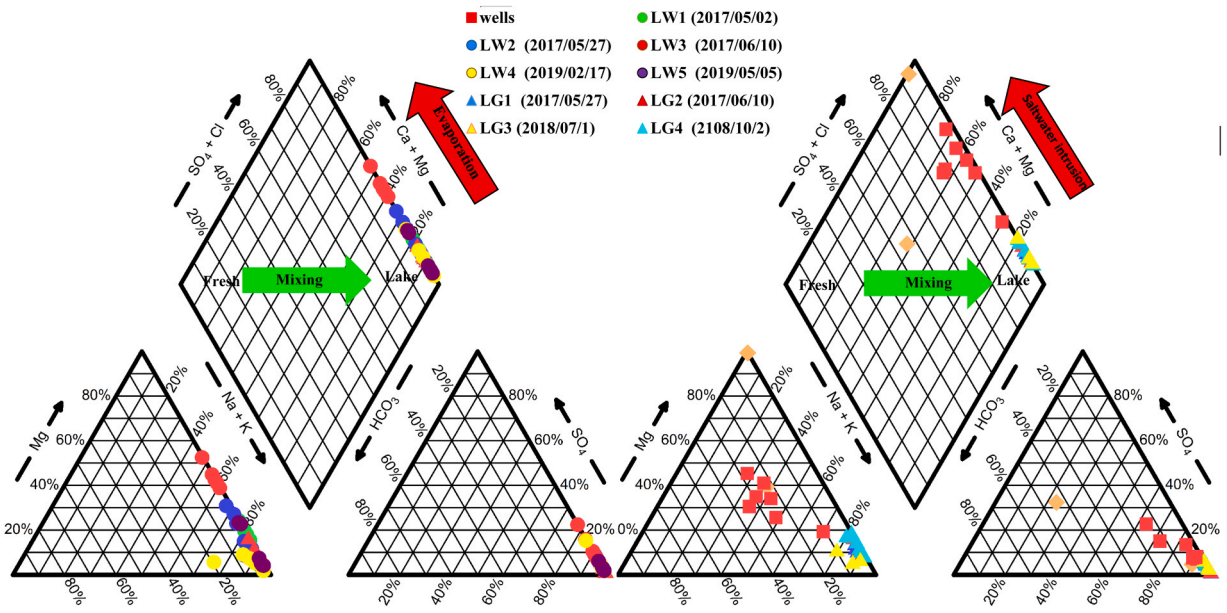

Fig. 5. Piper diagram of (a) lake water, (b) the groundwater below lake bed, and water of the wells and springs in the study area.

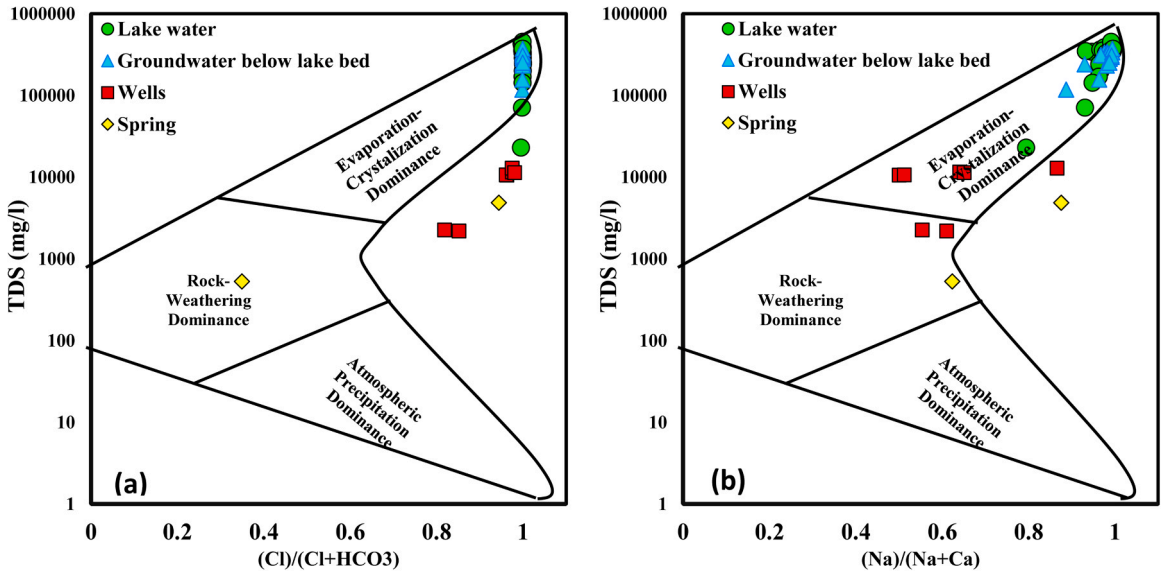

Fig. 6. Gibbs diagrams of the water samples in the Bakhtegan Lake area. **(a)** TDS vs.$Cl^-/(Cl^- + HCO_3^-)$; **(b)** TDS vs. $Na^+/(Na^+ + Ca^{2+})$ diagrams.

evaporation-crystallization on the chemical evolution of brine. Consequently, this process leads to a TDS concentration that is 12.8 times higher than that of actual seawater. The wells and one of the springs also demonstrate a distinct intrusion trajectory of lake water, particularly near the coast. Additionally, another spring and two well samples located far from the shoreline align with the water-rock interaction end-member, suggesting that the composition of major ions was primarily influenced by natural factors such as rock weathering. The results from the Gibbs diagram confirm that the Bakhtegan Lake samples are predominantly controlled by evaporation-crystallization, as expected. From a climatological perspective, intense radiation, significant evaporation rates, and minimal rainfall contribute to brine concentration.

The ratio of Na^+ to Cl^- and the relationship between Na^+ and Cl^- are crucial factors for determining the sources of these ions. If both ions originate from the dissolution of halite, the Na^+/Cl^- ratio should be equal to 1. However, if the ratio deviates from 1, it suggests that other sources contribute to the presence of these ions (Gil-Márquez et al., 2017; Jia et al., 2020). Figs. 7a and 7b demonstrate that all samples align with the halite dissolution line (1:1 relationship line). Specifically, for the March and May samples, sodium increases proportionally with chloride, indicating a common origin for these two ions (Fig. 7.a). This suggests that halite dissolution elevates both Na^+ and Cl^- concentrations during the early stages of evaporation. In contrast, the higher concentrations of Cl^- relative to Na^+ in the June samples indicates conservative behavior of Cl^- due to evapoconcentration processes. Furthermore, it suggests a decrease in Na^+ and Cl^- concentrations in solution during the later stages of evaporation due to halite precipitation. It is worth noting that approximately 74% of the surface bed of Bakhtegan and Tashk Lakes are covered by pure salt and clay salt crusts (Mohammadi, 2020). This implies that evaporation primarily leads to halite accumulation in the deeper parts of the lakes. In the process of dissolution, highly soluble minerals dissolve first while less soluble salts remain in solid form. Consequently, after a dissolution-evaporation cycle, water contains ions derived from highly soluble salts (Drever, 1997). Therefore, it can be inferred that halite dissolution is the primary source of sodium and chloride in the lake.

The molar Ca^{2+}/Na^+ against Mg^{2+}/Na^+ plots and HCO_3^-/Na^+ against Mg^{2+}/Na^+ end-member diagrams, proposed by Gaillardet et al. (1999), are used to differentiate the sources of ions resulting from carbonate weathering, evaporate dissolution, and silicate weathering in an area with complex lithology (Jiang et al., 2015; Zong-Jie et al., 2018; Liu et al., 2021; Wu et al., 2020; Shen et al., 2021). The primary sources of ions in water are categorized into evaporite dissolution (such as halite and gypsum), silicate weathering (including Ca-plagioclase, feldspar, and olivine), and carbonate rock (such as calcite, aragonite, and dolomite) (Li et al., 2020b).

Different types of rocks undergo weathering processes that result in distinct combinations of ions being released into a solution. For example, Ca^{2+} and Mg^{2+} primarily originate from the weathering of carbonates, evaporites, and silicates, while Na^+ and K^+ come from the weathering of both silicates and evaporites. HCO_3^- is derived from silicates and carbonates, while Cl^- and SO_4^{2-} are sourced from evaporites (Chen et al., 2002).

Here, all samples taken from the brine lake water and below the lake bed underwent evaporate dissolution, as shown in Figs. 7c and 7d. This indicates that the evaporation process was dominant. Wells and spring samples were found to be situated between the carbonate and evaporate end-members in Fig. 7c and d, suggesting that brine intrusion into adjacent aquifers resulted in groundwater salinization.

According to Xiao et al. (2012), the Mg^{2+} content remains constant during salt precipitation or soil salt leaching in the initial stages of evaporation. Therefore, the Mg^{2+}/Ca^{2+} versus Mg^{2+}/Na^+ ratios were used to differentiate between evaporation and soil salt leaching processes in certain regions (Xiao et al., 2012; Gao et al., 2017). Based on the Mg^{2+}/Ca^{2+} versus Mg^{2+}/Na^+ diagram shown in

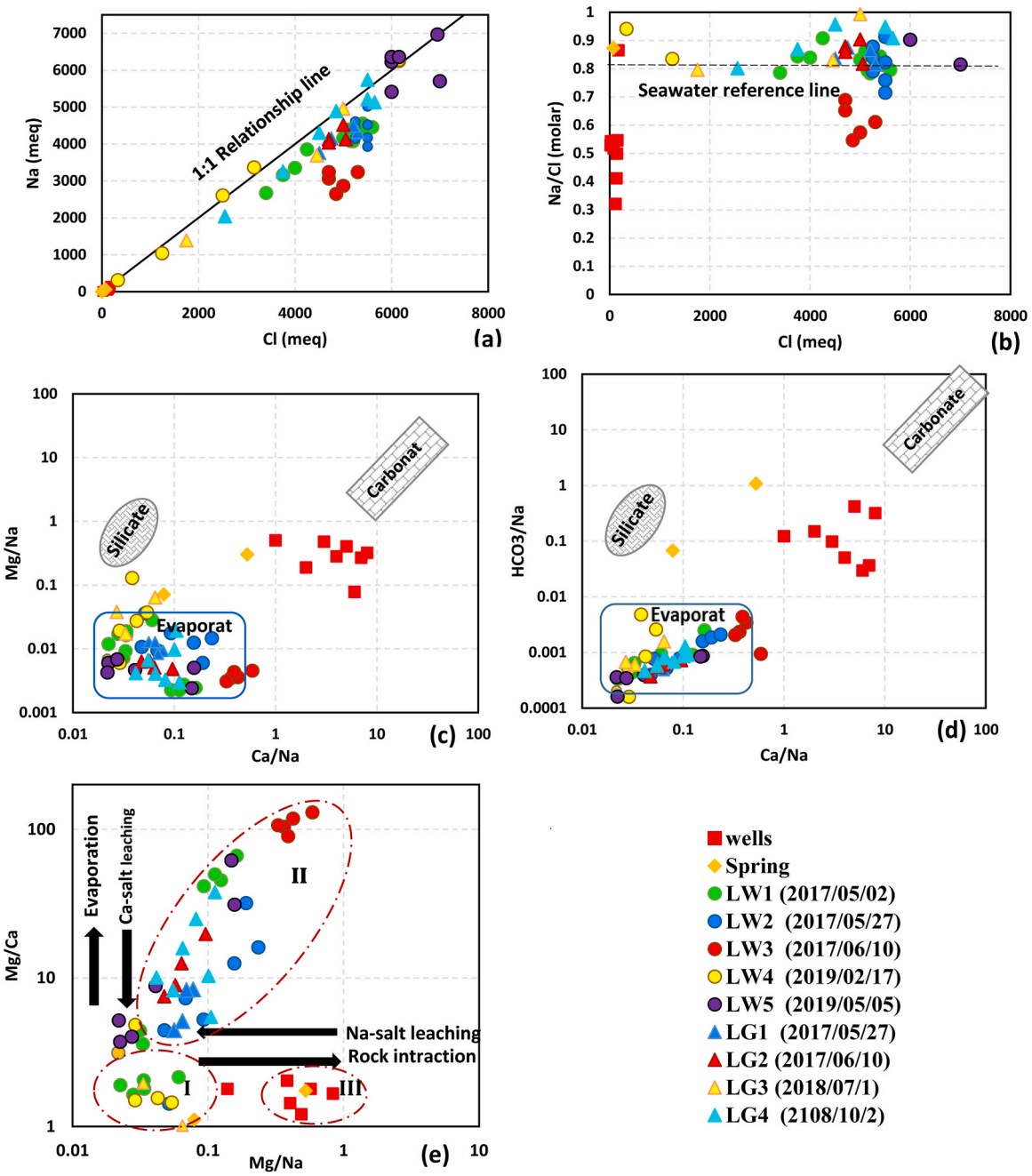

Fig. 7. (a) Na^+ versus Cl^-, (b) Na^+/Cl^- versus Cl^-, (c) Mg^{2+}/Na^+ versus Ca^{2+}/Na^+, (d) HCO_3^-/Na^+ versus Ca^{2+}/Na^+ and (e) Mg^{2+}/Ca^{2+} versus Mg^{2+}/Na^+diagrams. The end member compositions of carbonate, silicate and evaporite in Figs. c and d are from Gaillardet et al. (1999).

Fig. 7e, three groups can be identified among the water samples:

1) The first group consists of lake water samples with low ratios of both Mg^{2+}/Ca^{2+} and Mg^{2+}/Na^+ during the May and March sampling periods, indicating the dominance of salt leaching during the early stages after rainfall.
2) The second group includes lake water and the brine below lake bed samples with high ratios of Mg^{2+}/Ca^{2+} and low ratios of Mg^{2+}/Na^+, suggesting the dominance of evaporation during the evaporation process.
3) The third group comprises well and spring samples with low Mg^{2+}/Ca^{2+} ratios and high Mg^{2+}/Na^+ ratios, indicating the dominance of rock interactions.

Overall, these findings offer substantiation for the attainment of solutes through the process of evaporation evolution. However, it is important to note that the early stages of evaporation are influenced by the leaching of Na-salt, which impacts the compositions of the lake water samples.

4.5. Major, minor ions and minerals evolution

The evolution of major and minor ions and minerals was also examined in this study. Chloride was used as a measure of evaporation, and the behavior of major ions, minor ions, and TDS were investigated during changes in Cl^- levels. Fig. 8 displays bivariate plots showing the relationship between Cl^- and major ions (Na^+, Mg^{2+}, Ca^{2+}, K^+, SO_4^{2-} and HCO_3^-), minor ions (Li^+, Rb^+, $Cs^+$and Sr^{2+}), and TDS, as well as seawater evaporation trajectories (Fontes and Matray, 1993). The TDS showed a strong correlation (r^2 = 0.91) with Cl^- (Fig. 8i). The concentrations of Na^+ and Cl^- increased over time, but decreased during the final stages of evaporation in samples collected in mid-June 2017 (Fig. 8b). According to Eugster and Maglione (1979), high levels of Cl^- indicate the

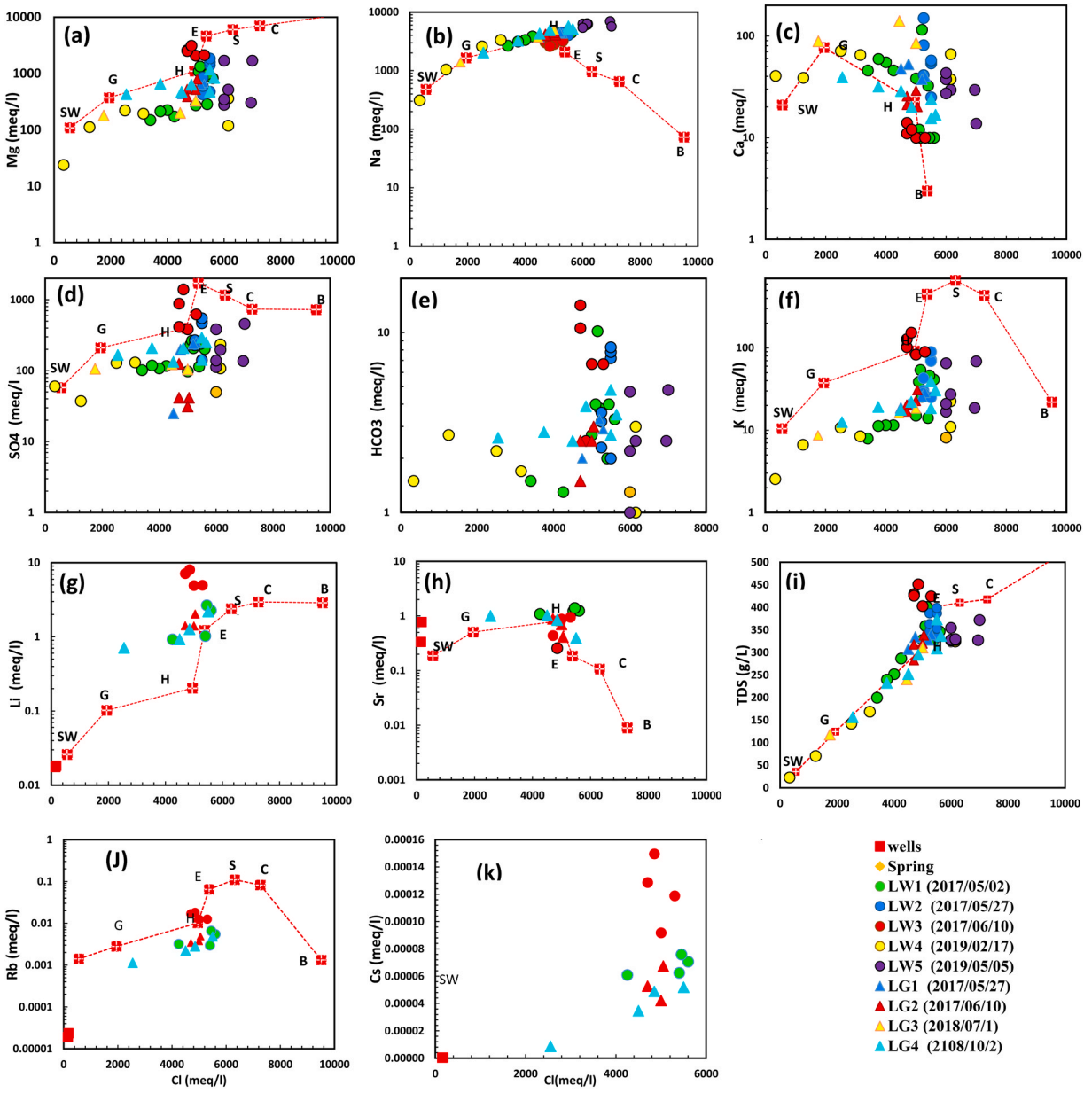

Fig. 8. Major and minor ions and TDS vs. Cl^- as a function of the evaporation process. The red dashed line represents the evolution of seawater ions during evaporation. SW: Seawater, G: Gypsum, H: Halite, E: Epsomite, S: Sylvite, C: Carnallite, B: Bischofite (Fontes and Matray, 1993).

evapotranspiration process because Cl^- is elevated during water body evaporation and is only removed during the last stages when halite minerals precipitate. The concentrations of Mg^{2+}, SO_4^{2-}, HCO_3^-, K^+, Li^+, $Rb^+$and Cs^+ showed significant increase with Cl^- from May to June, suggesting continuous reactions with evaporates (Fig. 8a, d, e, f, g, j, and k). Mg^{2+} and K^+ exhibited a strong relationship ($r^2 = 0.94$) due to their conservative behavior in solution and their presence in Mg-K salt (potash), found in highly evaporated water with an evaporation degree exceeding 50 (Shalev et al., 2018).

Furthermore, the dissolved ions of Li^+, $Rb^+$and Cs^+ in brine exhibit a strong correlation with Cl^- (as shown in Fig. 8g, j, and k). This suggests that Li^+, Rb^+ and Cs^+ ions remain relatively stable in highly concentrated water. On the other hand, Ca^{2+} and Sr^{2+} ions show a decrease during the evapoconcentration process due to the precipitation of carbonate minerals from the solution. This forms the first chemical divide, with Ca^{2+} being the first to be removed from the water (Fig. 8c) (refer to Section 4.5.2). Additionally, Sr^{2+} is known to substitute for Ca^{2+} in the calcite mineral lattice (Fig. 8h). The behavior of major and minor ions indicates that almost all samples follow a similar trend as the seawater evaporation trajectory (SET). Therefore, samples in the early stages of evaporation tend to precipitate gypsum, while samples with a higher degree of evaporation in June are closer to halite precipitation in SET.

4.5.1. Spencer triangle

In this study, the Spencer triangle was utilized to enhance the differentiation of the geochemical evolution of brine concentration resulting from evaporation (e.g., Spencer, 2000; Lowenstein et al., 2016; Campodonico et al., 2019; Li et al., 2020) (Fig. 9). The triangle represents the ternary system Ca^{2+}- SO_4^{2-} - Alkalinity based on the "chemical divides" model proposed by Hardie and Eugster (1970) for predicting the water evolution trajectory (Jones and Deocampo, 2003).

Since alkaline-earth carbonate minerals are primarily precipitated from solutes, this model determines the water composition during evaporation processes as a sequence of chemical divides, starting with calcite mineral precipitation. Consequently, in the Spencer triangle, chemical divides from calcite towards sulfate and calcite towards gypsum define three distinct sub-triangles for saline waters: neutral, alkaline, and Ca–Cl type (Fig. 9). Each zone is named based on the principal solutes removed in the final solution.

The lake water is distributed in the neutral fields on the Spencer triangle (Fig. 9). In March and early May, the lake water samples shift towards the Ca^{2+}- SO_4^{2-} axis, resulting in the precipitation of gypsum. As time progresses, especially in late May and June, the lake water samples evolve towards the SO_4^{2-} apex. The lake water, which undergoes progressive evaporation, becomes enriched in SO_4^{2-} content and moves towards the deposition of K-Mg sulfate minerals (Fig. 9).

4.5.2. SI

The SI values of carbonate minerals (calcite, dolomite, magnesite, aragonite, and huntite), sulfate minerals (gypsum, anhydrite, epsomite, glauberite, goergeyite, and mirabilite), and chloride minerals (halite and sylvite) as a function of TDS concentrations are shown in Fig. 10. The SI values of all the studied minerals clearly increase as TDS increases, indicating an evolution trend. Among the carbonate minerals, calcite, dolomite, magnesite, aragonite, and huntite were found to be in an oversaturated state in both lake water

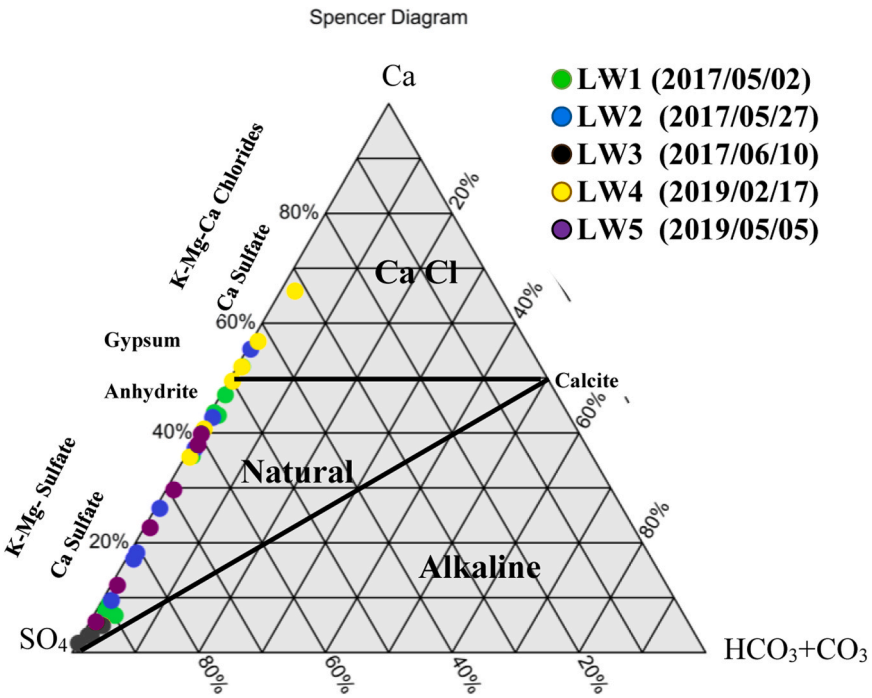

Fig. 9. Spencer triangles for the forecasting solute evolution pathways in the Ca^{2+}- SO_4^{2-}- (HCO_3^- + CO_3^{2-}) system.

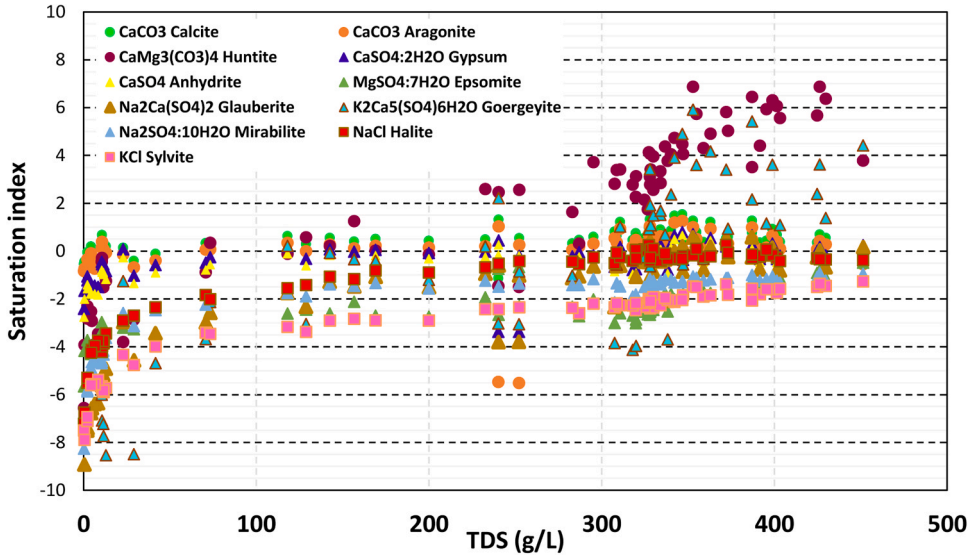

Fig. 10. Saturation index of minerals in the Bakhtegan Lake associated water samples.

and the brine below the lake bed samples. This suggests that precipitation of carbonate minerals has occurred due to the supersaturation of Ca and Mg carbonates in these samples. Consequently, the precipitation of carbonate minerals resulted in a decrease in Ca^{2+} and HCO_3^- concentrations in the solution.

Regarding sulfate minerals, based on the SI values, the lake water and brine below lake bed samples were found to be at a saturation state ($-0.5 < SI > 0.5$) with respect to gypsum, anhydrite, and glauberite, particularly in samples with TDS greater than 300000 mg/L. However, they were found to be at an unsaturated state with respect to epsomite and mirabilite.

Georgeyite precipitated in samples with high TDS. Gypsum, anhydrite, and glauberite were found to be in almost perfect equilibrium with the lake water. Therefore, it appears that these minerals are controlling the precipitation and dissolution processes. Among the chloride minerals, halite was found to be unsaturated in samples with TDS values less than 300000 mg/L. As TDS increased

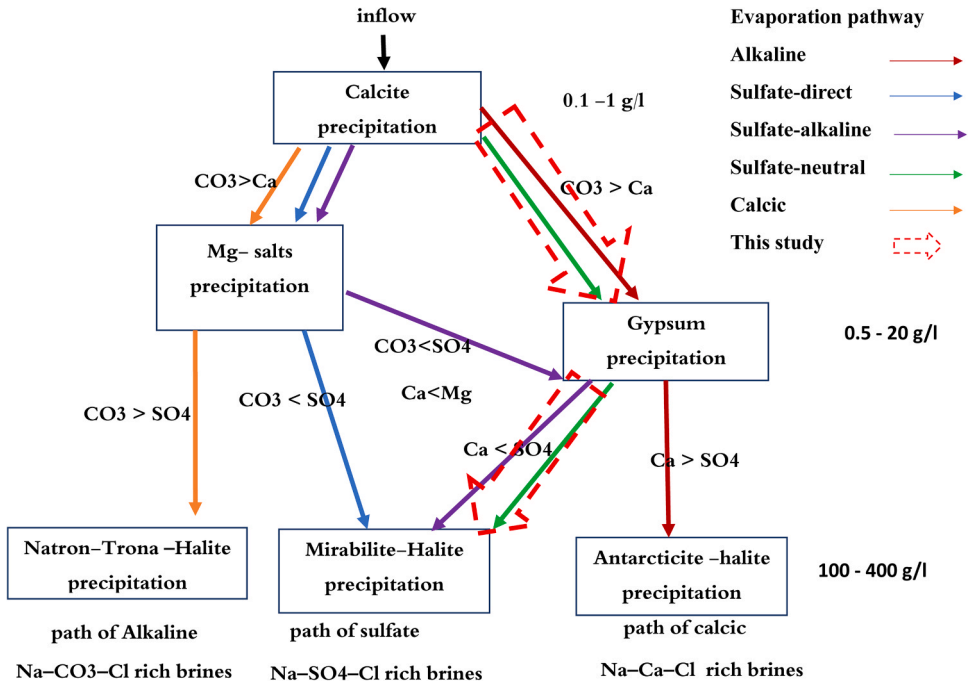

Fig. 11. Brine evolution diagram showing probable the Bakhtegan Lake evolution pathways of inflow waters (modified from Hardie and Eugster, 1970; Risacher and Fritz, 2009).

due to evaporation, the halite SI indicated equilibrium with the solution phase. On the other hand, sylvite remained unsaturated even in the final stage of evaporation. It is worth noting that minerals at their saturation state, mainly in the early stage of evaporation, had negative SI values, suggesting continuous dissolution of gypsum, anhydrite, halite, epsomite, and sylvite. As time goes on, this leads to an increase in the concentrations of Cl^-, Na^+, K^+ and SO_4^{2-}. However, halite precipitation in the final stage of evaporation will cause a decrease in Cl^- and Na^+ concentrations. In the well and spring samples, calcite and dolomite were found to be at saturation state, while the other minerals were unsaturated.

4.5.3. *Evolution pathway of the Bakhtegan Lake*

The evolution pathway of the Bakhtegan Lake, as proposed by Hardie and Eugster in 1970, is shown in Fig. 11. The pathway describes the chemical changes that occur in the lake's waters during evaporation. Four different evolutionary pathways are considered: path of alkaline, path of sulfate-alkaline (direct or indirect paths), path of sulfate-neutral, and path of calcic. The composition of the inflow waters of the Bakhtegan Lake appears to be related to the path of sulfate-neutral. During evaporation, the chemical composition of water changes as follows: Alk $< Ca^{2+}$ and $SO_4^{2-} >$Alk $+ Ca^{2+}$. This is due to the precipitation of calcite, which causes an increase in Ca^{2+}concentration and a decrease in alkalinity. In the next stage of evolution, Bakhtegan Lake has a higher concentration of SO_4^{2-} compared to Ca^{2+}, leading to gypsum precipitation. The chemical features of brines indicate further evolution towards deposition. Therefore, solution in the Bakhtegan Lake continues to evolve until it reaches its final composition of Na-Mg-SO_4-Cl, which is represented by mirabilite-halite in Fig. 11.

4.6. *Geochemical evolution modeling*

Geochemical evolution modeling is a process that involves the study of water evolution in a closed lake. This process is influenced by various factors such as the composition of inflow, selective elimination of solutes, and precipitation of minerals (Eugster and Smith, 1965; Hardie and Eugster, 1970; Eugster and Jones, 1979; Eugster, 1980). Brine evolution modeling focuses on the transformation of inflow waters into brine, which is regulated by brine concentration and evaporate precipitation. To simulate the brine evolution, a forward simulation was conducted at a temperature of 25°C and P_{CO2} of $10^{-3.4}$ using the PHREEQC software with Pitzer's database (Risacher and Clement, 2001). The simulation results are presented in two parts: the concentration factor (CF) for solutes content (upper part of Fig. 12) and the amounts of precipitated mineral phases (lower part of Fig. 12). For this study, a lake water sample collected in June, with the highest evaporation degree and TDS content of 451000 mg/L, was used as the input water for the model (Fig. 12). The existing lake water content was concentrated through continuous removal of water while allowing precipitation of gypsum, halite, epsomite, kieserite, and carnallite.

In the evaporation model, the lake water becomes saturated with gypsum. The concentrations of K^+ and Mg^{2+}, Cl^- gradually increase until reaching a CF of 3.7. These solutes behave as conservative ions before starting to decrease due to the precipitation of halite, kieserite, and carnallite (Fig12). On the other hand, Na^+, Ca^{2+}, SO_4^{2-}, and especially Ca^{2+}, participate in the precipitation of calcite, gypsum, and halite (Fig. 12b).

In this model, calcite precipitated in the previous stage, and the increase in SI calcite was supported by previous studies conducted by Möller and De Lucia (2020). Gypsum became saturated initially, but eventually became unsaturated due to evaporation. Subsequently, halite, kieserite, and carnallite appeared with concentration factors of 3.4, 3.7, and 5.4, respectively. The results obtained from the lake water with a concentration factor greater than 20 were deemed unreliable due to the high concentration of the sample. The assemblage of chloride and sulfate minerals in the predicted sequence of evaporate modeling indicates that extreme evaporative concentrations have an effect on lake water composition and mineral evolution similar to that of seawater evolution. However, during field investigations, halite minerals were found in the lake's sediments while kieserite and carnallite were not observed.

5. Conclusions

The time series data of the inundation lake in the past 47 years reveals a significant decrease in the size of lake water bodies in the last 12 years, specifically from 2007 to 2019. Typically, these lakes reach their maximum size in May during the wet years and dry up during the summer months. For instance, Bakhtegan Lake's water surface area has decreased from 512 km^2 in May 1973 to only 29 km^2 in May 2019, transforming it into a seasonal lake between 2007 and 2019. The available hydrometric station on the river indicates that the water body area is directly influenced by the inflow of water from the river. Interestingly, the results suggest that precipitation is not the main factor contributing to this sharp decrease in lake area. Instead, reduction in groundwater water level due to overexploitation by pumping wells and the construction of two new dams play a more dominant role than precipitation.

In order to gain a comprehensive and systematic understanding of the chemical compositions of the Bakhtegan Lake water and the factors that control its hydrochemistry, a total of 64 water samples were collected from the lake, the brine below the lake bed, springs, and wells in the adjacent aquifers. The main findings are as follows: The dominant water type in the lake is Na^+- Cl^-. Analysis of major and trace ions reveals a significant increase in SO_4^{2-}, Mg^{2+}, K^+, Li^+, Rb^+ and Cs^+ ions in the water samples with high levels of Cl^-. On the other hand, Ca^{2+} and Sr^{2+} show a decrease due to the evapo-concentration process and precipitation of carbonate minerals. The major and minor ions in the water samples align with the seawater evaporation trajectory, indicating that samples with high evaporation undergo halite precipitation on the SET line. The Na–Cl diagram demonstrates that halite dissolution is the primary source of major ions in both lake water and the brine below the lake bed. Various chemical signature diagrams, such as Gibbs and Na-normalized ratio end-member, suggest that evaporation processes control the chemistry of the lake water. The ratios of Mg^{2+}/Na^+versus Mg^{2+}/Ca^{2+}

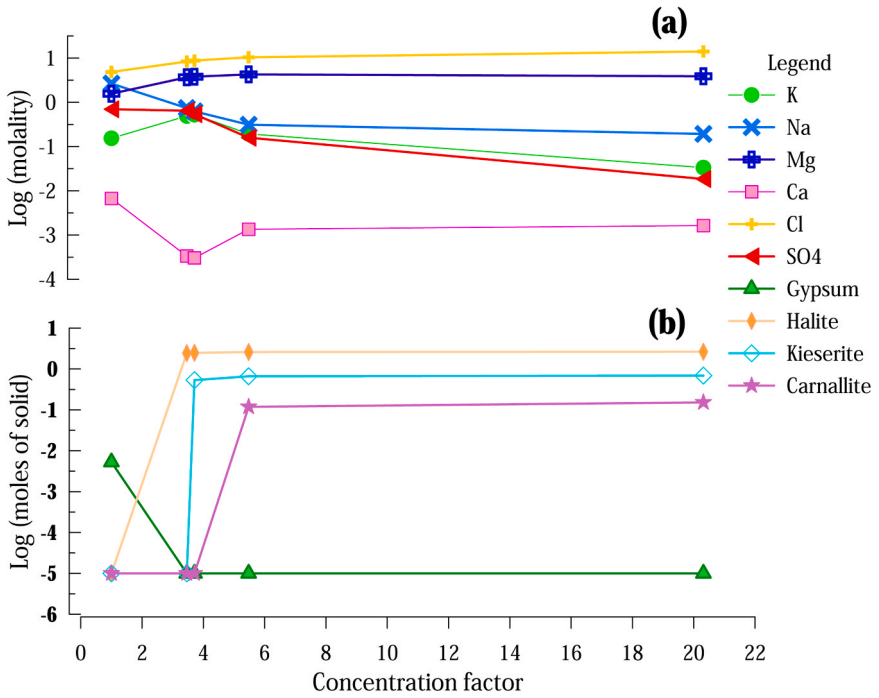

Fig. 12. (a) Major ions precipitation and (b) mineral precipitation sequence during evaporation of selected lake water sample.

highlight that salt leaching, particularly halite dissolution, is responsible for the elevated ion content after rainfalls in March and May. The Spencer diagram and evolutionary pathway indicate that the lake water tends towards the SO_4^{2-} apex, leading to the deposition of K-Mg sulfate minerals as evaporation progresses. Saturation index analysis reveals that carbonate minerals in the water samples precipitate, while samples with TDS levels exceeding 300000 mg/L are found to be in equilibrium with gypsum, anhydrite, glauberite, and halite. Lastly, according to a brine evolution model and simulated evaporation sequence, halite, epsomite, kieserite, and carnallite minerals are precipitated in the final stages of evaporation. The salinity enhancement of the lake water and the brine below the lake bed resulted in the flow direction being from the lake to all the coastal aquifers, such that the wells near the shoreline were shut down. Some of the heavy metals in the lake water and the brine below the lake bed are greater than the maximum concentration level. The transfer of these contaminants to coastal aquifers threats the life of people using the agricultural products in the future. It is recommended to monitor the salinity and the heavy metals of the Bakhtegan Lake environment.

CRediT authorship contribution statement

Sjoerd van der Zee: Writing – review & editing, Supervision, Resources, Project administration, Funding acquisition. **Ezzat Raeisi:** Writing – review & editing, Validation, Supervision, Resources, Project administration, Methodology, Investigation, Funding acquisition, Data curation, Conceptualization. **Maryam Vahidipour:** Writing – review & editing, Writing – original draft, Visualization, Validation, Software, Methodology, Investigation, Formal analysis, Data curation, Conceptualization.

Declaration of Competing Interest

The authors declare that they have no known competing financial interests or personal relationships that could have appeared to influence the work reported in this paper.

Data Availability

Data will be made available on request.

Acknowledgment

The authors sincerely appreciate the support of Shiraz University for this research. We also acknowledge the partial support provided by the Netherlands Organization for Scientific Research (NWO), which is partly funded by the Dutch Ministry of Economic Affairs and the Ministry of Infrastructure and Environment, as well as the partners of the Dutch Water Nexus consortium, under the NWO (KWR, STWOA) contract 14299. We express our gratitude to Dr. Fabien Magri from Freie Universität Berlin for his editing and

comments, which greatly improved our manuscript. The authors would also like to acknowledge Ms. Farahtaj Bahadori from Shiraz University for her assistance with the chemical analyses of the water samples. Lastly, we extend our thanks to all those who provided field work assistance, particularly Mr. Solymani from the Environmental Protection Organization and master student Mr. Ebrahim Mohammadi.

Appendix A. Supporting information

Supplementary data associated with this article can be found in the online version at doi:10.1016/j.ejrh.2024.101714.

References

Adams, K.D., Sada, D.W., 2014. Surface water hydrology and geomorphic characterization of a playa lake system: implications for monitoring the effects of climate change. J. Hydrol. 510, 92–102. https://doi.org/10.1016/j.jhydrol.2013.12.018.

APHA, 1998. Standard Methods for the Examination of Water and Wastewater, 20th edn. American Public Health Association, Washington.

Berberian, M., 1995. Master blind thrust faults hidden under the Zagros folds: active basement tectonics and surface morphotectonics. Tectonophysics 241, 193–224. https://doi.org/10.1016/0040-1951(94)00185-C.

Brantley, S.L., Crerar, D.A., Moller, N.E., Weare, J.H., 1984. Geochemistry of a modern marine evaporite; Bocana de Virrila, Peru. J. Sediment. Res. 54 (2), 447–462. https://doi.org/10.1306/212F843B–2B24-11D7-8648000102C1865D.

Campodonico, V.A., Dapeña, C., Pasquini, A.I., Lecomte, K.L., Piovano, E.L., 2019. Hydrogeochemistry of a small saline lake: assessing the groundwater inflow using environmental isotopic tracers (Laguna del Plata, Mar Chiquita system, Argentina). J. South Am. Earth Sci. 95, 102305 https://doi.org/10.1016/j.jsames.2019.102305.

Cao, H., Han, L., Liu, Z., Li, L., 2021. Monitoring and driving force analysis of spatial and temporal change of water area of Hongjiannao Lake from 1973 to 2019. Ecol. Inform. *61*, 101230 https://doi.org/10.1016/j.ecoinf.2021.101230.

Chen, J., Wang, F., Xia, X., Zhang, L., 2002. Major element chemistry of the Changjiang (Yangtze River). Chem. Geol. 187, 231–255. https://doi.org/10.1016/S0009-2541(02)00032-3.

Deutsch, W.J., 2020. Groundwater Geochemistry: Fundamentals and Application to Contamination. CRC, Boca Raton. https://doi.org/10.1201/9781003069942.

Drever J.I. 1997. The Geochemistry of Natural Waters: Surface and Groundwater Environments 3 rd Edition. Prentice Hall, Upper Saddle River. New Jersey. USA.436 pp.

Eugster, H.P., 1980. Geochemistry of evaporitic lacustrine deposits. Ann. Rev. EarthPlanet. Sci. 8, 35–63. https://doi.org/10.1146/annurev.ea.08.050180.000343.

Eugster, H.P., Maglione, G., 1979. Brines and evaporites of the Lake Chad basin,Africa. Geochim. Et. Cosmochim. Acta 43, 973–981. https://doi.org/10.1016/0016-7037(79)90087-5.

Eugster, H.P., Smith, G.I., 1965. Mineral equilibria in the Searles Lake evaporites,California. J. Pet. 6, 473–522. https://doi.org/10.1093/petrology/6.3.473.

Fan, Q., Lowenstein, T.K., Wei, H., Yuan, Q., Qin, Z., Shan, F., Ma, H., 2018. Sr isotope and major ion compositional evidence for formation of Qarhan Salt Lake, western China. Chem. Geol. 497, 128–145. https://doi.org/10.1016/j.chemgeo.2018.09.001.

Fontes, J.C., Matray, J.M., 1993. Geochemistry and origin of formation brines from the Parisbasin, France.1.brines associated with triassic salts. Chem. Geol. 109, 149175 https://doi.org/10.1016/0009-2541(93)90068-t.

Fotooli, B., 2002. Bakhtegan Management Integrated Plan Studies. Environmental Protection Agency, 157p (In Persian).

Franco, M.G., Arnold, Y.J.P., Santamans, C.D., Steinmetz, R.L.L., Tassi, F., Venturi, S., Jofré, C.B., Caffe, P.J., Córdoba, F.E., 2020. Chemical and isotopic features of Li-rich brines from the Salar de Olaroz, Central Andes of NW Argentina. J. South Am. Earth Sci. 103, 102742 https://doi.org/10.1016/j.jsames.2020.102742.

Gaillardet, J., Dupré, B., Louvat, P., Allègre, C.J., 1999. Global silicate weathering and CO2 consumption rates deduced from the chemistry of large rivers. Chem. Geol. 159 (1), 3–30. https://doi.org/10.1016/S0009-2541(99)00031-5.

Gao, Z., Lin, Z., Niu, F., Luo, J., Liu, M., Yin, G., 2017. Hydrochemistry and controlling mechanism of lakes in permafrost regions along the Qinghai-Tibet Engineering Corridor, China. Geomorphology 297, 159–169. https://doi.org/10.1016/j.geomorph.2017.09.020.

Gibbs, R.J., 1970. Mechanisms controlling world water chemistry. Science 170 (3962), 1088–1090. https://doi.org/10.1126/science.170.3962.1088.

Gil-Márquez, J.M., Barberá, J.A., Andreo, B., Mudarra, M., 2017. Hydrological and geochemical processes constraining groundwater salinity in wetland areas related to evaporitic (karst) systems. A case study from Southern Spain. J. Hydrol. 544, 538–554. https://doi.org/10.1016/j.jhydrol.2016.11.062.

Han, D.M., Song, X.F., Currell, M.J., Yang, J.L., Xiao, G.Q., 2014. Chemical and isotopic constraints on evolution of groundwater salinization in the coastal plain aquifer of Laizhou Bay, China. J. Hydrol. 508, 12–27. https://doi.org/10.1016/j.jhydrol.2013.10.040.

Hardie, L.A., Eugster, H.P., 1970. The evolution of closed-basin brines. Mineral. Soc. Am. Spec. Publ. 3, 273–290.

Ismail, M.A., Waqas, M., Ali, A., Muzzamil, M.M., Abid, U., Zia, T., 2022. Enhanced index for water body delineation and area calculation using Google Earth Engine: a case study of the Manchar Lake. J. Water Clim. Change 13 (2), 557–573. https://doi.org/10.2166/wcc.2021.282.

Jia, H., Qian, H., Zheng, L., Feng, W., Wang, H., Gao, Y., 2020. Alterations to groundwater chemistry due to modern water transfer for irrigation over decades. Sci. Total Environ. 717, 137170 https://doi.org/10.1016/j.scitotenv.2020.137170.

Jiang, L., Yao, Z., Liu, Z., Wang, R., Wu, S., 2015. Hydrochemistry and its controlling factors of rivers in the source region of the Yangtze River on the Tibetan Plateau. J. Geochem. Explor. 155, 76–83. https://doi.org/10.1016/j.gexplo.2015.04.009.

Jones, B.F., Deocampo, D.M., 2003. Geochemistry of saline lakes. TrGeo 5, 605. https://doi.org/10.1016/j.scitotenv.2020.137170.

Khosravi, R., Zarei, M., Bigalke, M., 2018. Characterizing major controls on spatial and seasonal variations in chemical composition of surface and pore brine of Maharlu Lake, southern Iran. Aquat. Geochem. 24 (1), 27–54. https://doi.org/10.1007/s10498-018-9329-y.

Levy, D.B., Amrhein, C., 2011. Geochemical evolution of hypersaline cave pools, Guadalupe Mountains, New Mexico. Chem. Geol. 290 (1-2), 60–66. https://doi.org/10.1016/j.chemgeo.2011.08.012.

Li, R., Liu, C., Xu, H., Jiao, P., Hu, Y., Fan, L., Sun, X., 2020. Genesis of Glauberite sedimentation in Lop Nur salt lake-constraints from thermodynamic simulation of the shallow groundwater in the Tarim River basin, China. Chem. Geol. 537, 119461 https://doi.org/10.1016/j.chemgeo.2019.119461.

Liu, J., Peng, Y., Li, C., Gao, Z., Chen, S., 2021. Characterization of the hydrochemistry of water resources of the Weibei Plain, Northern China, as well as an assessment of the risk of high groundwater nitrate levels to human health. Environ. Pollut. 268, 115947 https://doi.org/10.1016/j.envpol.2020.115947.

Liu, Z., Yao, Z., Wang, R., 2018. Automatic identification of the lake area at Qinghai–Tibetan plateau using remote sensing images. Quat. Int. https://doi.org/10.1016/j.quaint.2018.10.023.

Löffler, H., 1961. Beiträge zur Kenntnis der Iranischen Binnengewässer II. Int. Revue ges. Hydrobiol, 46 (3), 309–406. https://doi.org/10.1002/iroh.19610460304.

Lowenstein, T.K., Dolginko, L.A., García-Veigas, J., 2016. Influence of magmatic-hydrothermal activity on brine evolution in closed basins: Searles Lake, California. GSA Bull. 128 (9-10), 1555–1568. https://doi.org/10.1130/B31398.1.

Maghrebi, M., Noori, R., Partani, S., Araghi, A., Barati, R., Farnoush, H., Torabi Haghighi, A., 2021. Iran's groundwater hydrochemistry. Earth Space Sci. 8 (8), e2021EA001793 https://doi.org/10.1029/2021EA001793.

McFeeters, S.K., 1996. The use of the normalized difference water index (NDWI) in the delineation of open water features. Int. J. Remote Sens. 17 (7), 1425–1432. https://doi.org/10.1080/01431169608948714.

Meredith, K.T., Hollins, S.E., Hughes, C.E., Cendón, D.I., Hankin, S., Stone, D.J.M., 2009. Temporal variation in stable isotopes (18O and 2H) and major ion concentrations within the Darling river between Bourke and Wilcannia due to variable flows, saline groundwater influx and evaporation. J. Hydrol. 378 (3-4), 313–324. https://doi.org/10.1016/j.jhydrol.2009.09.036.

Micklin, P., 2016. The future Aral Sea: hope and despair. Environ. Earth Sci. 75, 844 doi:https://doi.org/10.1007/s12665-016-5614-5.

Mohammadi, E., 2020. Hydrology and Wind Erosion Potential of Tashk and Bakhtegan Lakes. Masters thesis. Shiraz University, Shiraz, Iran.

Möller, P., De Lucia, M., 2020. The impact of Mg2+ ions on equilibration of Mg-Ca carbonates in groundwater and brines. Geochemistry *80* (2), 125611. https://doi.org/10.1016/j.chemer.2020.125611.

Noori, R., Maghrebi, M., Mirchi, A., Tang, Q., Bhattarai, R., Sadegh, M., Madani, K., 2021. Anthropogenic depletion of Iran's aquifers. Proc. Natl. Acad. Sci. 118 (25), e2024221118 https://doi.org/10.1073/pnas.2024221118.

Otálora, F., Criado-Reyes, J., Baselga, M., Canals, A., Verdugo-Escamilla, C., García Ruiz, J.M., 2020. Hydrochemical and mineralogical evolution through evaporitic processes in Salar de Llamara Brines (Atacama, Chile). ACS Earth Space Chem. 4 (6), 882–896. https://doi.org/10.1021/acsearthspacechem.0c00085.

Parkhurst, D.L., Appelo, C.A.J., 1999. PHREEQC 2.15. A Computer Program for Spe-ciation, Batch-Reaction, One-Dimensional Transport and Inverse Geochemical Calculation. Water-Resources Investigation Report99-4295.

Parkhurst, D.L. and Appelo, C.A.J., 2013. Description of Input and Examples for Phreeqc Version 3: A Computer Program for Speciation, Batch-reaction, One-dimensional Transport, and Inverse Geochemical Calculations (No. 6-A43). US Geological Survey. https://doi.org/10.3133/tm6A43.

Piper, A.M., 1944. A graphic procedure in the geochemical interpretation of water analyses. Eos, Trans. Am. Geophys. Union 25 (6), 914–928. https://doi.org/10.1029/TR025i006p00914.

Ramsar Convention, 2023. The List of Wetlands of International Importance (the Ramsar List). http://www.ramsar.org/sites/default/files/documents/library/sitelist.pdf.

Risacher, F., Clement, A., 2001. A computer program for the simulation of evaporation of natural waters to high concentration. Comput. Geosci. 27, 191–201. https://doi.org/10.1016/S0098-3004(00)00100-X.

Risacher, F., Fritz, B., 2009. Origin of salt and brine evolution of Bolivian and Chilean Salars. Aquat. Geochem. 15 (1–2), 123–157 hattps://doi.org/10.1007/s10498-008-9056-.

Scuderi, L.A., Laudadio, C.K., Fawcett, P.J., 2017. Monitoring playa lake inundation in the western United States: modern analogues to late-Holocene lake level change. Quat. Res. 73, 48–58. https://doi.org/10.1016/j.yqres.2009.04.004.

Shalev, N., Lazar, B., Köbberich, M., Halicz, L., Gavrieli, I., 2018. The chemical evolution of brine and Mg-K-salts along the course of extreme evaporation of seawater–an experimental study. Geochim. Et. Cosmochim. Acta 241, 164–179. https://doi.org/10.1016/j.gca.2018.09.003.

Shen, B., Wu, J., Zhan, S., Jin, M., Saparov, A.S., Abuduwaili, J., 2021. Spatial variations and controls on the hydrochemistry of surface waters across the Ili-Balkhash Basin, arid Central Asia. J. Hydrol., 126565 https://doi.org/10.1016/j.jhydrol.2021.126565.

Spencer, R., 2000. Sulfate Minerals in Evaporite Deposits. In: In: Alpers, C., Jambor, J., Nordstrom, D. (Eds.), Sulfate Minerals, Reviews in Mineralogy and Geochemistry,vol. 40. Mineralogical Society of America and Geochemical Society, Washington DC, pp. 173–192 https://doi.org/10.2138/rmg.2000.40.3.

Stallard, R., Edmond, J., 1983. Geochemistry of the Amazon: 2. The influence of geology and weathering environment on the dissolved load. J. Geophys. Res. 88 (C14), 9671–9688. https://doi.org/10.1029/JC088iC14p09671. Oceans (1978–2012.

Torabi Haghighi, A., Kløve, B., 2017. Design of environmental flow regimes to maintain lakes and wetlandsin regions with high seasonal irrigation demand. Ecol. Eng. 100, 120–129. https://doi.org/10.1016/j.ecoleng.2016.12.015.

Ullah, I., Aslam, B., Shah, S.H.I.A., Tariq, A., Qin, S., Majeed, M., Havenith, H.B., 2022. An integrated approach of machine learning, remote sensing, and GIS data for the landslide susceptibility mapping. Land *11* (8), 1265. https://doi.org/10.3390/land11081265.

Vahidipour, M., Raeisi, E., Van Der Zee, S.E., 2021. Active saltwater intrusion of shrinking Bakhtegan-Thask Lakes in South Iran threatens the freshwater resources of coastal aquifers. J. Hydrol. Reg. Stud. 34, 100790 https://doi.org/10.1016/j.ejrh.2021.100790.

Vahidipour, M., Raeisi, E., van der Zee, S., E., 2022. Potentially toxic metals in sediments, lake water and groundwater of the Ramsar wetlands Bakhtegan–Tashk, South Iran: distribution and source assessment. Environ. Technol. Innov. *28*, 102789 https://doi.org/10.1016/j.eti.2022.102789.

Wang, Y., Shen, Y., Guo, Y., Li, B., Chen, X., Guo, X., Yan, H., 2022. Increasing shrinkage risk of endorheic lakes in the middle of farming-pastoral ecotone of Northern China. Ecol. Indic. *135*, 108523 https://doi.org/10.1016/j.ecolind.2021.108523.

Wu, H., Wu, J., Li, J., Fu, C., 2020. Spatial variations of hydrochemistry and stable isotopes in mountainous river water from the Central Asian headwaters of the Tajikistan Pamirs. CATENA 193, 104639. https://doi.org/10.1016/j.catena.2020.104639.

Xiao, J., Jin, Z.D., Zhang, F., Wang, J., 2012. Solute geochemistry and its sources of the groundwaters in the Qinghai Lake catchment, NW China. J. Asian Earth Sci. 52, 21–30. https://doi.org/10.1016/j.jseaes.2012.02.006.

Yechieli, Y., Wood, W.W., 2002. Hydrogeologic processes in saline systems: playas, sabkhas, and saline lakes. Earth Sci. Rev. 58 (3-4), 343–365. https://doi.org/10.1016/S0012-8252(02)00067-3.

Zhou, Y., Dong, J., Xiao, X., Liu, R., Zou, Z., Zhao, G., Ge, Q., 2019. Continuous monitoring of lake dynamics on the Mongolian Plateau using all available Landsat imagery and Google Earth Engine. Sci. Total Environ. 689, 366–380. https://doi.org/10.1016/j.scitotenv.2019.06.341.

Zhu, L., Ke, Y., Hong, J., Zhang, Y., Pan, Y., 2022. Assessing degradation of lake wetlands in Bashang Plateau, China based on long-term time series Landsat images using wetland degradation index. Ecol. Indic. *139*, 108903 https://doi.org/10.1016/j.ecolind.2022.108903.

Zong-Jie, L., Zong-Xing, L., Ling-Ling, S., Jin-Zhu, M., Yong, S., 2018. Environment significance and hydrochemical characteristics of supra-permafrost water in the source region of the Yangtze River. Sci. Total Environ. 644, 1141–1151. https://doi.org/10.1016/j.scitotenv.2018.07.029.